CHEMISTRY OF MATERIALS

Article

pubs.acs.org/cm

Mixed Matrix Membranes (MMMs) Comprising Exfoliated 2D Covalent Organic Frameworks (COFs) for Efficient CO_2 Separation

Zixi Kang,[†] Yongwu Peng,[†] Yuhong Qian,[†] Daqiang Yuan,[‡] Matthew A. Addicoat,[§] Thomas Heine,[§] Zhigang Hu,[†] Lincoln Tee,[†] Zhengang Guo,[†] and Dan Zhao*[,†]

[†]Department of Chemical and Biomolecular Engineering, National University of Singapore, 4 Engineering Drive 4 117585, Singapore

[‡]State Key Laboratory of Structural Chemistry, Fujian Institute of Research on the Structure of Matter, Chinese Academy of Sciences, Fuzhou, 350002 Fujian, China

[§]School of Engineering and Science, Jacobs University Bremen, Campus Ring 1, 28759 Bremen, Germany

Supporting Information

ABSTRACT: Two water-stable covalent organic frameworks (COFs) named NUS-2 and NUS-3 having two-dimensional (2D) layered structures with different pore sizes were synthesized. These COFs were exfoliated into nanosheets and even monolayers with high aspect ratio. They were subsequently blended with commercial polymers poly(ether imide) (Ultem) or polybenzimidazole (PBI) into mixed matrix membranes (MMMs) exhibiting highly homogeneous textures due to the excellent compatibility between COF fillers and polymer matrixes. Thanks to the selective gas sorption properties of the porous COF fillers, the prepared MMMs exhibited increased gas permeabilities with NUS-2@PBI demonstrating an excellent H_2/CO_2 permselectivity that exceeded the 2008 Robeson upper bound. Our approach of using exfoliated 2D COFs as porous fillers in MMMs paves a novel way toward the tailored synthesis of advanced composite membrane materials for clean energy and environmental sustainability.

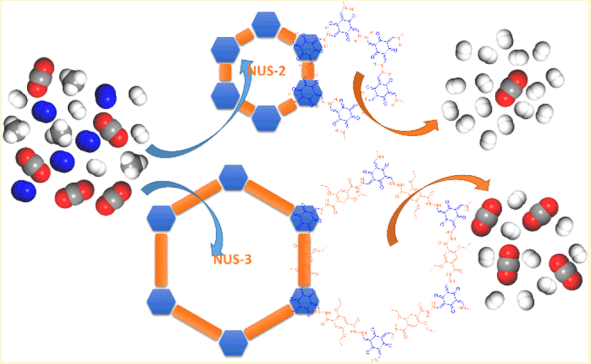

INTRODUCTION

Gas separation technologies, especially for CO_2 separation, have attracted increased attention recently because of their important applications in clean energy and environmental sustainability.[1,2] For example, natural gas contains a substantial amount of acidic gases such as CO_2 and H_2S that need to be removed to increase the heating value and prevent pipeline corrosion.[3] This process is called natural gas sweetening in which CO_2/CH_4 separation plays an important role. Another example is H_2/CO_2 separation which is a key step in H_2 purification and precombustion CO_2 capture from power plants.[4]

Membrane-based CO_2 separation has been greatly developed in recent years.[5−9] Compared to other CO_2 separation technologies such as amine scrubbing and pressure swing adsorption, membrane-based separation has the advantages of compact design, easy operation, low footprint, and scalability, meaning it can be employed independently or as a supplement to existing gas separation technologies in small chemical plants or off-shore applications where small but efficient gas separation is required.

Although several important achievements have been made in membrane morphology and module design, such as asymmetric hollow fiber membranes,[10] the defining component of membrane-based gas separation is still the membrane material itself. Polymeric materials have dominated this area since the initial concept of membrane-based gas separation because of their easy processability, decent performance, and low cost.[9] However, these materials suffer from the trade-off between permeability (separation throughput) and selectivity (separation efficiency), which can be depicted by the Robeson upper bounds.[11,12] Other major problems of polymeric materials include plasticization, fouling, and chemical and thermal instabilities.[13] Their inorganic counterparts such as ceramic membranes,[14] zeolite membranes,[15] carbon molecular sieve membranes,[16] and more recently metal−organic frameworks (MOFs) and zeolitic imidazolate frameworks (ZIFs) membranes[17−20] offer a much better balance between permeability and selectivity due to their well-defined porosities and rigid framework structures. However, their problems of brittleness and high cost confine the applications to only special cases where polymeric membranes are not able to meet the required specifications.[21] In order to combine the merits of both polymeric and inorganic membranes, mixed matrix membranes (MMMs) were invented by dispersing porous fillers into continuous polymeric matrixes hoping to increase the

Received: July 27, 2015
Revised: January 26, 2016
Published: February 17, 2016

DOI: 10.1021/acs.chemmater.5b02902
Chem. Mater. 2016, 28, 1277−1285

permeability and selectivity of the resulting membranes while preserving the properties of good mechanical strength and processability of the polymeric matrixes.[22−25] Polymeric matrixes are normally commercial rubbery and glassy polymers, and ideal porous fillers should have the properties of (1) excellent stability under working conditions, (2) high compatibility with polymeric matrixes, (3) selective gas permeation properties, and (4) nanosized morphology to prevent agglomeration and sedimentation. Zeolites were the first kind of porous filler used in MMMs.[26] However, poor compatibility between inorganic zeolites and organic polymers often leads to defects such as pin holes and sieve-in-a-cage structures that hurt the gas selectivity of the obtained MMMs.[27] Several zeolite surface modification studies have been reported trying to enhance the compatibility, but the improvement is only moderate.[22] Recently, there are several studies using MOFs and ZIFs as porous fillers in preparing MMMs with much better compatibilities due to the organic−inorganic hybrid structures of MOFs and ZIFs.[28−30] Nevertheless, it is quite challenging to prepare nanosized MOF or ZIF particles to prevent aggregation and sedimentation.[31] In addition, most MOFs and ZIFs have poor stabilities in wet and acidic conditions which are identical to the working conditions of CO_2 separation.[32] Therefore, the long-term stability of MOFs and ZIFs being used as fillers in MMMs for CO_2 separation still remains to be studied.

As a new member of the porous crystalline material family, covalent organic frameworks (COFs) are pure organic polymers composed of strong covalent bonds with light elements such as B, C, N, O, etc.[33,34] Unlike traditional polymers which are amorphous or semicrystalline, COFs are highly crystalline whose structures can be determined on the basis of powder crystal X-ray diffraction, or even single crystal X-ray[35] and electron[36] diffraction experiments. The crystallinity of COFs comes from the reversible covalent bond formation reactions (also known as dynamic covalent chemistry, DCC)[37] resulting in spontaneous correction of structural defects toward thermodynamically stable crystalline structures. COFs are normally constructed with rigid monomers which give them permanent porosities that have wide applications in storage, separation, catalysis, etc.[38,39] In addition, quite a large number of reported COFs have 2D layered structures that allow them to be exfoliated into multilayered or even single layered nanosheets with high aspect ratios and interesting properties.[40−43] In this study, we report the design and synthesis of two new COFs named NUS-2 and NUS-3 (NUS stands for National University of Singapore) with 2D layered structures and excellent water/acid stabilities. These COFs were exfoliated into nanosheets or even monolayers with high aspect ratios and used as fillers to prepare MMMs that were systematically evaluated for their CO_2 separation performance.

EXPERIMENTAL SECTION

Materials and Equipment. All chemicals and reagents are commercially available and used without purification. 1,3,5-Triformylphloroglucinol (TFP) and 2,5-diethoxy-terephthalohydrazide (DETH) were synthesized according to the published procedures.[42,44] Poly(ether imide) (Ultem) was kindly provided by SABIC (Saudi Basic Industries Corporation), and polybenzimidazole (PBI) was kindly provided by PBI performance products, Ins.

Fourier transform infrared spectroscopy (FTIR) spectra were obtained with a Bio-Rad FTS-3500 ARX FTIR spectrometer under N_2 atmosphere. Elemental analyses (C, H, and N) were performed on a Vario MICRO series CHNOS elemental analyzer. Solid-state nuclear magnetic resonance (NMR) data were collected on a Bruker Avance 400 MHz NMR spectrometer (DRX400) with cross-polarization magic-angle-spinning (CP/MAS). Powder X-ray diffraction (PXRD) patterns were obtained on a Bruker D8 Advance X-ray powder diffractometer equipped with a Cu sealed tube (λ = 1.54178 Å) at a scan rate of 0.02 deg s^{-1}. Thermogravimetric analyses (TGAs) were performed using a Shimadzu DTG-60AH in the temperature range 50−800 °C under flowing N_2 (50 mL min^{-1}) with a heating rate of 10 °C min^{-1}. Scanning electron microscopy (SEM) was conducted on a JEOL-JEM5600 Lab-SEM (15 kV) equipped with an energy dispersive spectrometer. Field-emission scanning electron microscopy (FE-SEM) was conducted on an FEI Quanta 600 SEM (20 kV) equipped with an energy dispersive spectrometer (EDS, Oxford Instruments, 80 mm2 detector). Samples were treated via Pt sputtering before observation. Field-emission transmission electron microscopy (FE-TEM) was conducted on a JEOL-JEM 2010F FE-TEM. Pure polymeric membranes and MMMs were imbedded within epoxy glue and sliced into disks for FE-TEM observation. Atomic force microscopy (AFM) was carried out by testing samples deposited on silica wafers using tapping mode with a Bruker Dimension Icon atomic force microscope.

Synthetic Procedures. *NUS-2.* A 10 mL Pyrex tube was charged with TFP (42.0 mg, 0.2 mmol), hydrazine hydrate (15 μL, 0.3 mmol), mesitylene/dioxane (1:1 v/v, 2 mL), and aqueous acetic acid (6 M, 0.2 mL). The mixture was sonicated for 2 min to get a homogeneous dispersion. The tube was then flash frozen at 77 K with a liquid N_2 bath and degassed by three freeze−pump−thaw cycles, sealed under vacuum, and heated at 120 °C for 3 days. The yielded red precipitate was collected by centrifugation and washed with anhydrous acetone, anhydrous tetrahydrofuran, and anhydrous ethanol, separately. The collected powder was then activated by solvent exchange with anhydrous methanol 3 times and dried at 120 °C under vacuum for 12 h to give a deep red powder with 82% isolated yield and a molecular formula of $(C_9H_6N_3O_3)_n$ (% calcd/found: C 52.95/52.70, H 2.96/2.86, N 20.58/20.45).

NUS-3. A 10 mL Pyrex tube was charged with TFP (42.0 mg, 0.2 mmol), DETH (84.0 mg, 0.3 mmol), *o*-DCB/dioxane (2:3 v/v, 2 mL), and aqueous acetic acid (6 M, 0.2 mL). The mixture was sonicated for 2 min to get a homogeneous dispersion. The tube was then flash frozen at 77 K with a liquid N_2 bath and degassed by three freeze−pump−thaw cycles, sealed under vacuum, and heated at 120 °C for 3 days. The yielded yellow precipitate was collected by centrifugation and washed with anhydrous acetone, anhydrous tetrahydrofuran, and anhydrous ethanol, separately. The collected powder was then activated by solvent exchange with anhydrous methanol 3 times and dried at 120 °C under vacuum for 12 h to give a deep yellow powder with 85% isolated yield and a molecular formula of $(C_9H_9N_2O_3)_n$ (% calcd/found: C 55.96/55.60, H 4.70/4.52, N 14.50/14.38).

NUS-2/NUS-3@Ultem. Ultem was heated at 150 °C under vacuum for 10 h to remove moisture and any adsorbed impurities. In a typical process to prepare MMMs, NUS-2 or NUS-3 (30, 60, and 90 mg, respectively) was added to chloroform (10 mL) to give suspension A, and Ultem (270, 240, and 210 mg, respectively) was dissolved in chloroform (2.5 mL) to give solution B. Suspension A was sonicated for 30 min using an ultrasonic homogenizer (Biobase, JY92-IIDN)

DOI: 10.1021/acs.chemmater.5b02902
Chem. Mater. 2016, 28, 1277−1285

followed by stirring for another 30 min. This cycle was repeated twice, and then $^1/_3$ volume of solution B was added followed by another sonication−stirring cycle. After that, the rest of solution B was added, and the total solution was sonicated and stirred once more to give the membrane casting solution, which was casted onto a flat glass substrate followed by slow vaporization of solvent to give the final MMM.

NUS-2/NUS-3@PBI. PBI was heated at 180 °C under vacuum for at least 12 h to remove moisture and any adsorbed impurities. The MMMs of NUS-2/NUS-3@PBI were prepared according to the published procedure.[45] Briefly, PBI (2 g) was first dissolved in *N*-methyl-2-pyrrolidone (NMP, 60 mL) by stirring at 120 °C for 48 h, followed by filtration after cooling down to room temperature. NUS-2 or NUS-3 (15, 30, and 45 mg, respectively) was added into *N*,*N*-dimethylformamide (DMF, 2.25, 2, and 1.75 mL, respectively), and the sonication−stirring cycle described previously was carried out twice. The obtained suspension was mixed with PBI solution (~5 mL) followed by another sonication−stirring cycle to give the membrane casting solution, which was casted onto a flat glass substrate and dried at 75 °C under vacuum for 12 h. After being cooled down to room temperature, the membrane was peeled off and further dried at 200 °C under vacuum for 1 day to give the final MMM.

The thickness of obtained MMMs was measured by a micrometer caliper (50−100 μm). The COF loading of MMMs was calculated by the weight of COFs divided by the total weight of COFs and polymers.

Gas Sorption Measurements. Gas sorption isotherms were measured up to 1 bar using a Micromeritics ASAP2020 surface area and pore size analyzer. Before the measurements, the sample (~50 mg) was degassed under reduced pressure (<10^{-2} Pa) at 150 °C for 12 h. UHP grade He, N_2, and CO_2 were used for all the measurements. Oil-free vacuum pumps and oil-free pressure regulators were used to prevent contamination of the samples during the degassing processes and isotherm measurements. The temperatures of 77, 273, and 298 K were maintained with a liquid nitrogen bath, with an ice−water bath, and under room temperature, respectively. The Brunauer−Emmett−Teller (BET) surface areas were calculated from N_2 adsorption isotherms at 77 K. Pore size distribution data were also calculated from the N_2 adsorption isotherms at 77 K based on nonlocal density functional theory (NL-DFT) model in the Micromeritics ASAP2020 software package (assuming cylinder pore geometry).

Single Gas Permeation Tests. The single gas (H_2, CH_4, and CO_2) permeabilities in MMMs were tested using a variable pressure constant volume gas permeation cell technique. The setup of gas permeation cell and testing procedures have been described previously.[46] For MMMs containing Ultem, tests were done on multiple membranes (2−3) with the same COF loading to get the average values. Each test was performed after the sample was degassed to a pressure of 1−10 mTorr, and the system reached thermal equilibrium after around 5 h. The operating temperature was maintained at 35 °C, and the upstream gas gauge pressure was set at 2, 3.5, and 5 bar, respectively. The gas permeability was calculated from the rate of pressure increasing (dp/dt) at a steady state according to eq 1

$$P = \frac{273 \times 10^{10}}{760} \frac{VL}{AT(p_2 \times 76/14.7)} \left(\frac{dp}{dt}\right) \quad (1)$$

where P is the membrane gas permeability in barrer (1 barrer = 1×10^{-10} cm^3 (STP) cm cm^{-2} s^{-1} cm Hg^{-1}), V represents the volume of the downstream reservoir (cm^3), L refers to the membrane thickness (cm), A is the effective membrane area (cm^2), T is the operating temperature (K), and p_2 indicates the upstream pressure (psia).

The ideal permselectivity of component i over component j was calculated on the basis of eq 2

$$\alpha_{(i/j)} = \frac{P_i}{P_j} \quad (2)$$

Mixed Gas Permeation Tests. The equimolar H_2/CO_2 mixed gas permeabilities in MMMs were tested using the same gas permeation cell setup described previously coupled with a Shimadzu gas chromatograph (GC-2014) equipped with HayeSep Q columns. Each test was performed after the sample was degassed to a pressure of 1−10 mTorr, and the system reached thermal equilibrium after around 12 h. The operating temperature was maintained at 35 °C, and the upstream gas gauge pressure was set at 5 bar. The mixed gas permeability was calculated from the rate of pressure increasing (dp/dt) in the downstream side at a steady state according to eq 3

$$P_i = \frac{273 \times 10^{10}}{760} \frac{y_i VL}{AT(x_i p_2 \times 76/14.7)} \left(\frac{dp}{dt}\right) \quad (3)$$

where P_i is the membrane mixed gas permeability of component i in barrer (1 barrer = 1×10^{-10} cm^3 (STP) cm cm^{-2} s^{-1} cm Hg^{-1}), x_i and y_i represent the molar fractions of component i in the upstream and downstream, respectively, V represents the volume of the downstream reservoir (cm^3), L refers to the membrane thickness (cm), A is the effective membrane area (cm^2), T is the operating temperature (K), and p_2 indicates the upstream pressure (psia).

The mixed gas separation factor was calculated on the basis of eq 4,

$$S_{(i/j)} = \frac{y_i/y_j}{x_i/x_j} \quad (4)$$

RESULTS AND DISCUSSION

Structure and Morphology of COFs. Most COFs are synthesized through condensation reactions between diol and boronic acids or esters affording high crystallinities due to the reversibility of these reactions.[34] However, these COFs are also vulnerable toward hydrolysis due to the same reason for highly reversible condensation reactions.[47] This drawback greatly limits their applications in CO_2 separation given the wet and corrosive working conditions. Banerjee's group has reported a family of water-stable COFs, whose stability comes from the irreversible enol−keto tautomerization that helps to lock the COFs into a more stable isomorph with increased resistance toward hydrolysis.[48,49] This approach has been successfully applied in synthesizing COFs with extraordinary stabilities in not just neutral aqueous solutions but even acidic ones.[50,51] In this study, we targeted our COF synthesis using similar chemistry to increase the long-term stabilities of COFs suitable for industrial CO_2 separation requirements.

By judicious selection of monomers and optimization of reaction conditions, two COFs named NUS-2 and NUS-3 were synthesized through aldehyde−amine condensation accompanied by enol−keto tautomerization locking them into more

DOI: 10.1021/acs.chemmater.5b02902
Chem. Mater. 2016, 28, 1277−1285

stable isomorphs (Figure 1). It is worth noting that NUS-2 has been reported as COF-JLU2[52] and ATFG-COF[53] during the

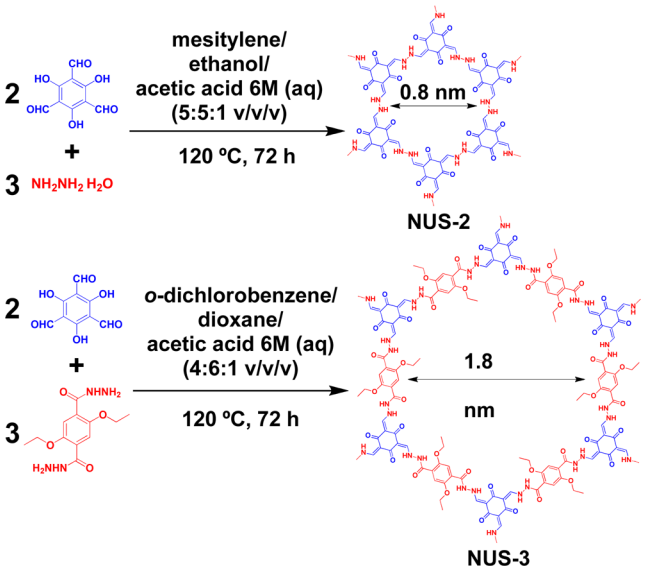

Figure 1. Synthetic procedure and idealized structures of 2D COFs NUS-2 and NUS-3.

preparation and revision of this paper. FTIR spectra indicated the disappearance of carbonyl stretching band of TFP (1643 cm^{-1}), while a series of new characteristic stretching bands at 1597, 1516, and 1284 cm^{-1} for NUS-2 and 1628, 1585, and 1192 cm^{-1} for NUS-3 arising from the C═O, C═C, and C—N stretching bands, respectively, were observed indicating condensation reactions and tautomerization (Figure S1).[48] The ^{13}C CP/MAS NMR spectra further confirmed the proposed chemical structures of NUS-2 and NUS-3, with the chemical shifts of keto-form carbonyl carbon at 191 ppm for NUS-2 and 192 ppm for NUS-3 (Figure S2).[48]

The 2D layered crystal structures of NUS-2 and NUS-3 were created with AuToGraFS[54] and optimized with SCC-DFTB[55] (Figure 2 and Table S1−S4). The interlayer distances are 3.3

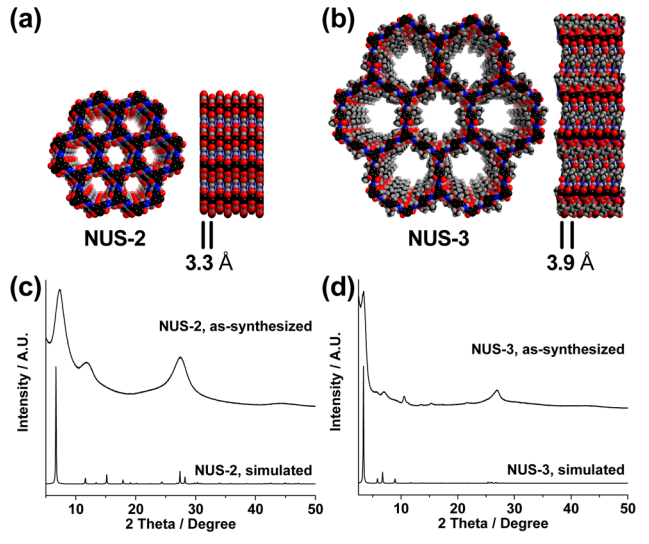

Figure 2. Simulated crystal structures of (a) NUS-2 and (b) NUS-3; PXRD patterns of (c) NUS-2 and (d) NUS-3.

and 3.9 Å for NUS-2 and NUS-3, respectively. Both COFs exhibit hexagonal channels of different diameters (0.8 nm for NUS-2 and 1.8 nm for NUS-3 measured through crystal models) that will play an important role in determining the gas sorption and permeation behaviors. Instead of being a perfect eclipsed AA stacking, NUS-2 has a slipped AA stacking which helps to reduce the pore size and make the channel wall corrugated resulting in benefits for selective gas sorption (*vide infra*). The proposed structure of NUS-2 agrees well with the reported results.[52,53] In NUS-3, the monolayer is not flat but slightly corrugated, which is probably because of the extra ethyl groups on the bridging unit leading to steric repulsion between layers. The experimental PXRD patterns of NUS-2 and NUS-3 match well with the ones simulated on the basis of the created crystal structures. The slightly broad PXRD peaks observed at higher angles of ∼24−28° for experimental data may arise from defects in the $\pi-\pi$ stacking between successive COF layers.[49]

As has been expected on the basis of our molecular design, both NUS-2 and NUS-3 exhibited excellent resistance toward hydrolysis. Their crystallinities were barely affected after being treated in boiling water and even in boiling acid solutions (pH = 5.5) for 1 week (Figure S3). In addition, they are thermally stable up to 300 °C as revealed by TGA curves (Figure S4). Such high hydrothermal and chemical stabilities make NUS-2 and NUS-3 excellent candidates as porous fillers in preparing MMMs that can sustain their integrity under the harsh working conditions of industrial CO_2 separation.

The morphology and size of as-synthesized NUS-2 and NUS-3 were studied by FE-SEM and FE-TEM. FE-SEM images show that NUS-2 and NUS-3 were crystallized in a uniform flower-like morphology with dimensions ranging from 2 to 5 μm (Figure S5). This flower-like morphology is identical to other COFs prepared using similar chemistry.[48,49] Each "flower" is composed of many ribbons with a length of 1−2 μm and a width of 50−100 nm. These ribbons can be easily detached into discrete layers with extremely small thickness under sonication in the process of membrane preparation, as revealed by the FE-TEM images (Figure S6). It needs to be pointed out that, during the preparation of MMMs reported in the literature, great efforts have been made in reducing the size of fillers to increase their compatibility with polymeric matrixes and prevent their agglomeration and sedimentation.[22] For NUS-2 and NUS-3 reported herein, the inherent nanosize makes them a good candidate as MMM fillers evidenced by the week-long stability of their suspensions without any visible sedimentation.

During the preparation of membrane casting solutions, NUS-2 and NUS-3 need to be suspended in organic solvents and sonicated for quite a long time. This experimental condition is identical to the method for the exfoliation of 2D materials[56−58] and COFs.[40] Inspired by this analogy, AFM was used to verify the morphology of NUS-2 and NUS-3 after sonication and stirring in DMF. It can be clearly seen that both COFs were exfoliated into nanosheets with a size of 50−100 nm and high aspect ratios (Figure 3). It is surprising to note that some nanosheet heights of NUS-2 and NUS-3 can be as low as ∼3.5 Å indicating monolayers which is unprecedented in the reported COF exfoliation studies.[40−43] The AFM phase images as well as larger scale AFM images and statistical distribution of COF nanosheet dimensions and heights can be found in the Supporting Information (Figures S7−S8, Table S5−S6), which prove that most COFs were exfoliated into nanosheets during the sonication step of membrane preparation. It is anticipated

DOI: 10.1021/acs.chemmater.5b02902
Chem. Mater. 2016, 28, 1277−1285

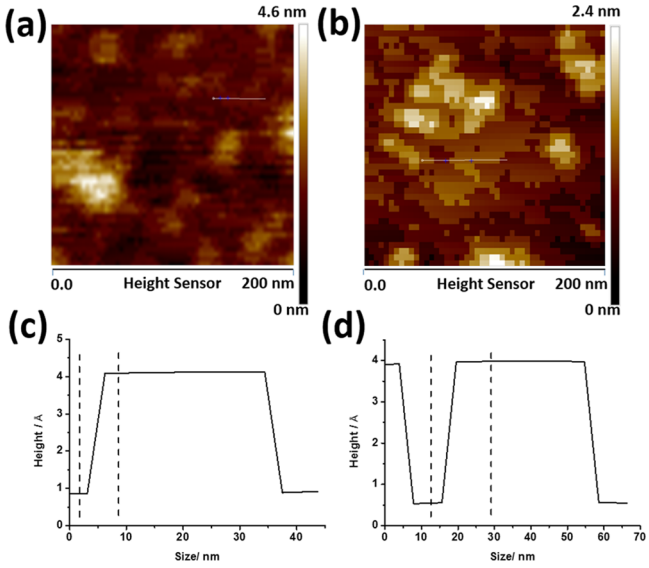

Figure 3. AFM images of sonicated (a) NUS-2 and (b) NUS-3 dispersed on Si wafer along with the cross-sectional height profiles of (c) NUS-2 and (d) NUS-3.

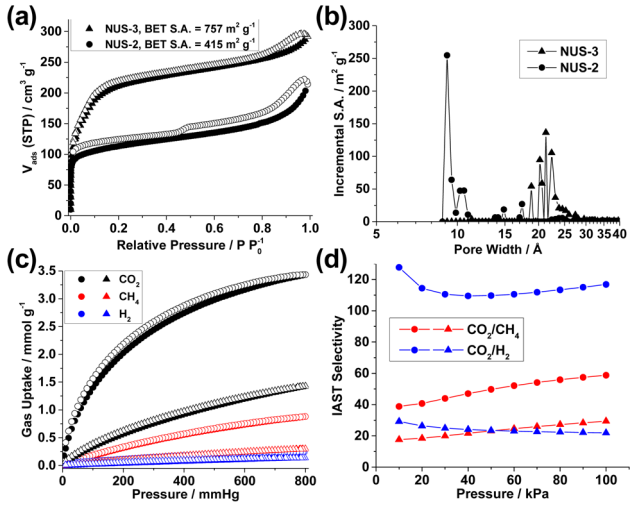

Figure 4. (a) N_2 sorption isotherms of NUS-2 and NUS-3 at 77 K; (b) pore size distribution of NUS-2 and NUS-3; (c) CO_2 (black), CH_4 (red), and H_2 (blue) sorption isotherms of NUS-2 and NUS-3 at 273 K; (d) CO_2/CH_4 (red) and CO_2/H_2 (blue) IAST selectivities of NUS-2 and NUS-3 at 273 K. NUS-2, circle; NUS-3, triangle; adsorption, closed; desorption, open.

that the nanosheet morphology of NUS-2 and NUS-3 can greatly increase their compatibility and stability within polymeric matrixes leading to MMMs with better structures and performance. To further confirm the structure of exfoliated COFs, the COF nanosheets in the solution after sonication were filtered onto a porous support (anodic aluminum oxide, AAO), and were further characterized by PXRD and FTIR (Figure S9). The crystallinity of original COFs was completely lost in the sonicated samples due to the exfoliation and disruption of stacking along the *c* direction.[42] The similar FTIR spectra between as-synthesized and exfoliated COFs prove the maintenance of in-phase structure and bond connection after exfoliation.

Porosity and Gas Sorption of COFs. The permanent porosity of NUS-2 and NUS-3 was assessed by measuring N_2 sorption isotherms at 77 K (Figure 4). Both COFs exhibit combined type I/IV isotherms indicating hybrid micro/mesoporous structures. The microporous structure (pore size less than 2 nm) is anticipated from the crystal models, while the mesoporous structure (pore size between 2 and 50 nm) may originate from the interstitial voids among COF nanoparticles as well as crystal defects. The surface area calculated on the basis of the BET model is 415 $m^2\ g^{-1}$ for NUS-2 and 757 $m^2\ g^{-1}$ for NUS-3, which are comparable to other 2D COFs with hexagonal channels such as DAAQ-TFP COF (365 $m^2\ g^{-1}$),[50] COF-LZU1 (410 $m^2\ g^{-1}$),[59] TpPa-1 (535 $m^2\ g^{-1}$),[48] etc. The higher BET surface area of NUS-3 compared to that of NUS-2 can be explained by the longer building units which is similar to the MOF analogues.[60,61] Pore size distribution data calculated on the basis of N_2 sorption isotherms reveal average pore sizes of 9 Å for NUS-2 and 21 Å for NUS-3, which agree well with the crystal models.

In order to evaluate the selective gas sorption properties of NUS-2 and NUS-3, various gas sorption isotherms (H_2, CH_4, and CO_2) were collected at 273 and 298 K, respectively (Figure 4, Figure S10). For both COFs, the uptake of CO_2 is much higher than that of other gases under the same test conditions. This behavior is identical to other porous materials and can be attributed to the stronger interactions between CO_2 and adsorbents.[62] In our case, the CO_2–adsorbent interactions are further strengthened due to the amino fragments in NUS-2 and NUS-3 that have high affinities toward CO_2 due to their basicity.[63] Compared to NUS-3 which can reversibly uptake 1.5 mmol g^{-1} of CO_2 at 273 K and 1 bar, the CO_2 uptake capacity of NUS-2 is even higher (3.5 mmol g^{-1}) despite its lower surface area. This is probably because of the reduced pore size of NUS-2 that increases the affinity toward CO_2.[64] Our hypothesis is confirmed by the isosteric heat of adsorption (Q_{st}), which can be used to quantitatively evaluate the adsorbate–adsorbent interactions. The Q_{st} for low-coverage CO_2 of NUS-2 is 28.2 kJ mol^{-1}, which is unambiguously higher than that of NUS-3 (22.2 kJ mol^{-1}) indicating a stronger CO_2–COF interaction (Figure S11).

The binary CO_2/CH_4 and CO_2/H_2 selectivities were calculated on the basis of the single gas isotherms using ideal adsorbed solution theory (IAST, Figure 4 and Table S7).[65] NUS-2 exhibited higher selectivities than NUS-3 because of its higher CO_2 uptake under similar conditions. The IAST CO_2/H_2 selectivity of NUS-2 at 273 K and 1 bar is 116.8, which is comparable to some of the best adsorbents for hydrogen purification.[66] This high IAST CO_2/H_2 selectivity of NUS-2 would make it an effective porous filler in preparing MMMs for H_2/CO_2 separation, which will be discussed in the later part.

Preparation and Characterization of MMMs. Two commercially available polymers, namely, Ultem (poly(ether imide)) and PBI (polybenzimidazole), were selected due to their good performance in gas separation.[67] MMMs were fabricated by casting stock solutions containing fully dissolved polymers and suspended COFs (10, 20, and 30 wt %, respectively). COFs were thoroughly sonicated and stirred during stock solution preparation to ensure homogeneity. On the basis of the previous AFM study, COFs were exfoliated into nanosheets or even monolayers during this operation. This can be confirmed from the PXRD patterns of MMMs in which the low-angle peaks of both NUS-2 and NUS-3 are missing in most MMMs indicating that COFs in MMMs have been exfoliated into nanosheets or even monolayers (Figure S12). This special

DOI: 10.1021/acs.chemmater.5b02902
Chem. Mater. 2016, 28, 1277–1285

nanosheet morphology of fillers is beneficial for good compatibility with the polymeric matrixes because of increased contact areas. In addition, enhanced gas separation performance has been demonstrated in MMMs containing nanosheet-like inorganic fillers and MOFs.[68−71] It is believed that aligning nanosheet fillers orthogonally to the gas concentration gradient direction will bring the maximum increase in gas separation performance of resulting MMMs.[70] In the reported studies, TEM and focused ion beam SEM (FIB-SEM) were used to characterize the dispersion and orientation of layered fillers in MMMs.[69,70] In this study, we have tried to characterize MMMs using FE-TEM (Figure S13). However, because of the similar contrast and chemical composition between COFs and polymers, we could not get conclusive evidence for the dispersion and orientation of COF fillers in MMMs yet. Nevertheless, some structural information can be revealed by the cross-sectional SEM images. COF-loaded MMMs exhibit plastic deformation featured by polymer veins (Figure 5 and Figures S14−S15) that have been reported previously in MMMs containing MOF nanocrystals. These polymer veins were attributed to strong interactions between MOF nanocrystals and polymeric matrixes,[72,73] indicating strong interactions between COFs and polymeric matrixes as well.

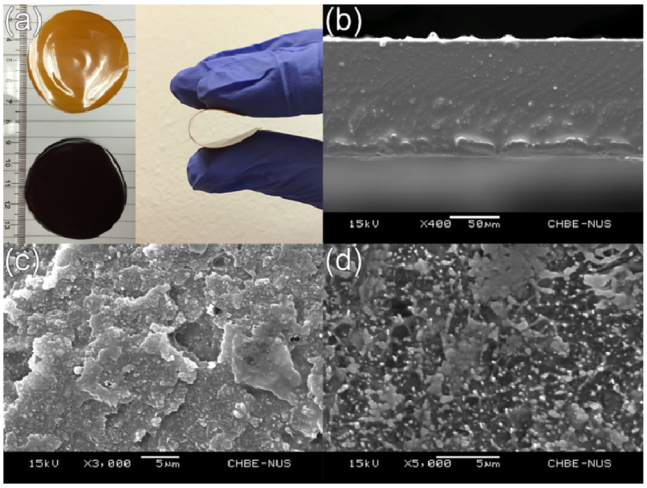

Figure 5. (a) Optical images of 20 wt %NUS-2@Ultem (brown) and 20 wt %NUS-3@Ultem (black); (b) cross-sectional SEM image of pure Ultem membrane; (c) cross-sectional SEM image of 20 wt % NUS-2@Ultem; (d) cross-sectional SEM image of 20 wt %NUS-3@Ultem.

Tests of Gas Permeation in MMMs. In order to evaluate the performance of prepared MMMs, single gas (H_2, CH_4, and CO_2) permeation tests were performed under various pressures (2, 3.5, and 5 bar, respectively). Unlike the selectivity defined in sorption-based separation which describes the difference of gas sorption ability, the selectivity defined in membrane-based separation emphasizes the difference of gas permeability, which is how fast the gas can penetrate through the membranes. In polymeric membranes, gas separation can be typically described using the solution−diffusion model, in which permeability **P** can be expressed by $\mathbf{P} = \mathbf{S} \times \mathbf{D}$ where **S** is the solubility of a particular gas in polymer and **D** is the diffusivity of that specific gas.[22] Gas solubility is controlled by the affinity of gas toward polymer and can be measured by gas sorption isotherms, while gas permeability is dominated by the free volume of polymer. Adding fillers into polymers can affect both **S** and **D**, while the affected trend may not always be the same. If the fillers are porous (like COFs in this case), **D** would be affected to a larger extent than **S** as the free volume of MMMs can be increased dramatically. This will be illustrated using CO_2/CH_4 and H_2/CO_2 gas pairs in the following discussion.

For the gas pair of CO_2/CH_4, whose separation is of paramount importance in natural gas sweetening, adding lower amounts (10 and 20 wt %) of COFs into Ultem increases both the solubility and diffusivity of CO_2, leading to a desired shift toward the upper-right corner in the chart of CO_2 permeability versus CO_2/CH_4 selectivity (Figure 6a,b and Table S8). The solubility increase is due to the higher affinity of CO_2 toward COFs, and the diffusivity increase is because of the increased free volume of MMMs caused by COFs. It needs to be pointed out that adding COFs also increases the permeability of CH_4 within MMMs, but to a smaller extent than CO_2 leading to an overall increase in CO_2/CH_4 selectivity. Compared to NUS-2@Ultem, NUS-3@Ultem has a comparable CO_2/CH_4 selectivity but a much larger CO_2 permeability (Figure 6b) because of the larger pore size of NUS-3 leading to faster gas diffusivity.

When a larger amount (30 wt %) of COFs was added, NUS-2@Ultem has a further increased CO_2 permeability but decreased CO_2/CH_4 selectivity, while NUS-3@Ultem has both decreased CO_2 permeability and CO_2/CH_4 selectivity. During the preparation of these Ultem MMMs with high COF loading, we noticed that it was very hard to get homogeneous membrane casting solutions because of the light density of COFs and low viscosity of polymer solutions. Therefore, we suspect that there might be some large domains in MMMs without COF fillings that caused the decreased gas permeation.

H_2/CO_2 separation is attracting ever-increasing attention nowadays due to its important role in H_2 purification and precombustion CO_2 capture.[4] The H_2/CO_2 separation performance of Ultem MMMs with low COF loading (10 and 20 wt %) exhibit a similar trend. For NUS-3@Ultem, the H_2/CO_2 selectivity decreases at a higher COF loading possibly due to the large pore size of NUS-3. MMMs perform even worse at a higher COF loading (30 wt %) which is identical to CO_2/CH_4 separation.

Because of its dense polymeric chain packing, PBI can be used to separate H_2 from CO_2 on the basis of molecular size difference.[67] In this study, another series of MMMs was prepared using PBI as the polymeric matrix. Although H_2 has a relatively low affinity toward COFs (small **S**), its diffusivity in NUS-3@PBI has been dramatically increased (extra-large **D**) because of the extra voids brought about by the porous COF filler, leading to a H_2 permeability that is ∼17-fold of that of the pure PBI membrane in 30 wt %NUS-3@PBI (increased **P**, Figure 6f and Table S9). During the single gas permeation tests, it is interesting to note that although the increase of H_2 permeability in NUS-2@PBI is only marginal, the CO_2 permeability actually decreased in a compariton to that of the pure PBI membrane, leading to an increase in the H_2/CO_2 selectivity. Most remarkably, the CO_2 permeability of 20 wt % NUS-2@PBI continues to decrease with increasing pressure, leading to a H_2/CO_2 selectivity of 31.4 surpassing the 2008 Robeson upper bound.[12] The decreased CO_2 permeability at higher pressures can be explained by the saturation of Langmuir sites based on dual sorption theory.[74] Because of its strong affinity toward CO_2, the added NUS-2 serves as extra Langmuir sites for CO_2 sorption leading to saturation under higher pressures and lower CO_2 permeability.

DOI: 10.1021/acs.chemmater.5b02902
Chem. Mater. 2016, 28, 1277−1285

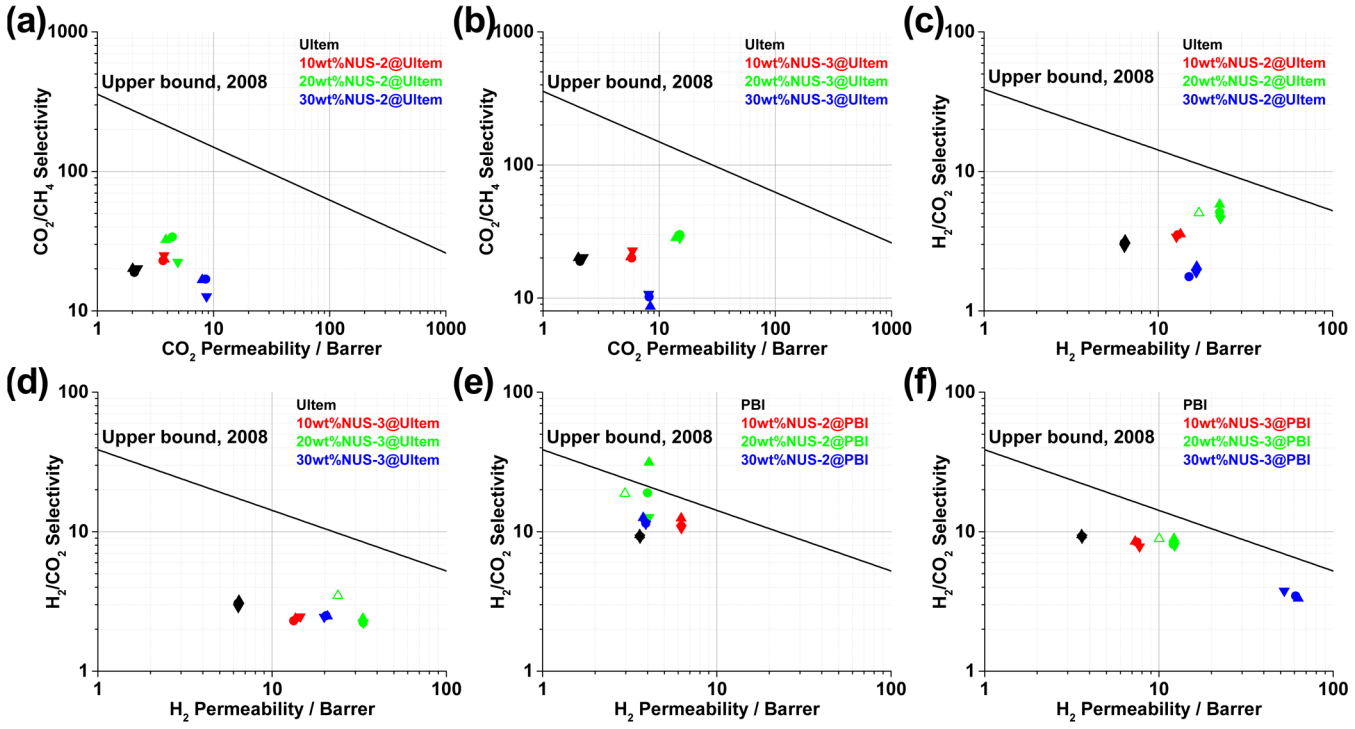

Figure 6. Single gas and mixed gas permeation properties of polymeric membranes and MMMs: (a) CO_2/CH_4 for NUS-2@Ultem, (b) CO_2/CH_4 for NUS-3@Ultem, (c) H_2/CO_2 for NUS-2@Ultem, (d) H_2/CO_2 for NUS-3@Ultem, (e) H_2/CO_2 for NUS-2@PBI, (f) H_2/CO_2 for NUS-3@PBI. Down triangle, 2 bar; circle, 3.5 bar; up triangle, 5 bar. Solid and hollow symbols represent single gas data and mixed gas data, respectively. Error bars are too small to be displayed. The 2008 Robeson upper bounds for CO_2/CH_4 and H_2/CO_2 separation are included to reflect state-of-the-art polymeric membrane performance.

An equimolar H_2/CO_2 mixed gas was used to evaluate the real gas separation performance of fabricated MMMs under 5 bar (Figure 6c–f). The measured gas separation factors for MMMs with 20 wt % COF loading (both NUS-2 and NUS-3) are compared to the calculated ideal selectivities (Table S10). Compared to single gas permeation tests, mixed gas permeation tests tend to give different results due to the competitive adsorption and diffusion of the binary gas components in the membrane. In this study, decreased H_2 permeabilities (20–30% decrease compared to single gas results) were observed in all membranes in the H_2/CO_2 mixed gas tests (Figure 6c–f and Table S10). This phenomenon can be attributed to the CO_2-favored adsorption in the COF-loaded MMMs, which reduces the diffusion of H_2 in the membranes due to pore blocking by adsorbed CO_2. For MMMs containing NUS-2 with small pores and strong affinity toward CO_2, such competition leads to reduced H_2/CO_2 selectivities: from 5.80 (single gas tests) to 5.04 (mixed gas tests) for NUS-2@Ultem, and from 31.40 (single gas tests) to 18.78 (mixed gas tests) for NUS-2@PBI. On the other hand, for MMMs containing NUS-3 with larger pores and weaker CO_2 affinity, the separation factors of H_2/CO_2 are not affected for NUS-3@PBI and even increased for NUS-3@Ultem (from 2.39 in single gas tests to 3.48 in mixed gas tests). This may due to the larger pore size and pore volume of NUS-3 that alleviated such competition between H_2 and CO_2 within membranes.

CONCLUSIONS

In summary, two water-stable covalent organic frameworks (COFs) named NUS-2 and NUS-3 having 2D layered structures and hexagonal channels with different pore sizes were successfully synthesized. They exhibited good thermal stability (up to 300 °C) and excellent resistance toward hydrolysis in both neutral and acidic conditions. They can be exfoliated into nanosheets or even monolayers under sonication and stirring, and were blended with commercial polymers poly(ether imide) (Ultem) and polybenzimidazole (PBI) into mixed matrix membranes (MMMs). Thanks to the good compatibility between COF fillers and polymeric matrixes, these MMMs have defect-free structures with good mechanical properties. The single gas permeability tests of H_2, CH_4, and CO_2, as well as the H_2/CO_2 mixed gas permeability tests, were carried out on the obtained MMMs to evaluate their performance in gas separation. Compared to the pure polymer membranes, our COF-containing MMMs exhibited increased gas permeabilities and/or selectivities. On the basis of the single gas tests, one of the MMMs (20 wt %NUS-2@PBI) exhibited a H_2/CO_2 perselectivity up to 31.4 under higher pressures which has surpassed the 2008 Robeson upper bound. The performance was slightly deteriorated in mixed gas tests due to the competitive adsorption and diffusion of H_2 and CO_2 in membranes. Our work demonstrates this for the first time using exfoliated nanosheet or even monolayer 2D crystalline COFs as fillers in the preparation of MMMs and has depicted a clear way toward the tailored synthesis of advanced composite membrane materials for their applications in clean energy and environmental sustainability.

ASSOCIATED CONTENT

Supporting Information

The Supporting Information is available free of charge on the ACS Publications Web site at The Supporting Information is available free of charge on the ACS Publications website at DOI: 10.1021/acs.chemmater.5b02902.

DOI: 10.1021/acs.chemmater.5b02902
Chem. Mater. 2016, 28, 1277–1285

Experimental procedures and additional figures and tables (PDF)

AUTHOR INFORMATION

Corresponding Author

*E-mail: chezhao@nus.edu.sg.

Author Contributions

Z.K., Y.P., and Y.Q. contributed equally to this work.

Notes

The authors declare no competing financial interest.

ACKNOWLEDGMENTS

This work is supported by National University of Singapore (CENGas R-261-508-001-646) and Singapore Ministry of Education (MOE AcRF Tier 1 R-279-000-410-112, AcRF Tier 2 R-279-000-429-112).

REFERENCES

(1) Figueroa, J. D.; Fout, T.; Plasynski, S.; McIlvried, H.; Srivastava, R. D. Advances in CO_2 capture technology - the U.S. Department of Energy's carbon sequestration program. *Int. J. Greenhouse Gas Control* **2008**, *2*, 9−20.

(2) Haszeldine, R. S. Carbon capture and storage: how green can black be? *Science* **2009**, *325*, 1647−1652.

(3) Chaemchuen, S.; Kabir, N. A.; Zhou, K.; Verpoort, F. Metal-organic frameworks for upgrading biogas *via* CO_2 adsorption to biogas green energy. *Chem. Soc. Rev.* **2013**, *42*, 9304−9332.

(4) Scholes, C. A.; Smith, K. H.; Kentish, S. E.; Stevens, G. W. CO_2 capture from pre-combustion processes-strategies for membrane gas separation. *Int. J. Greenhouse Gas Control* **2010**, *4*, 739−755.

(5) Baker, R. W. Future directions of membrane gas separation technology. *Ind. Eng. Chem. Res.* **2002**, *41*, 1393−1411.

(6) Bernardo, P.; Drioli, E.; Golemme, G. Membrane gas separation: a review/state of the art. *Ind. Eng. Chem. Res.* **2009**, *48*, 4638−4663.

(7) Merkel, T. C.; Lin, H. Q.; Wei, X. T.; Baker, R. Power plant post-combustion carbon dioxide capture: an opportunity for membranes. *J. Membr. Sci.* **2010**, *359*, 126−139.

(8) Du, N. Y.; Park, H. B.; Dal-Cin, M. M.; Guiver, M. D. Advances in high permeability polymeric membrane materials for CO_2 separations. *Energy Environ. Sci.* **2012**, *5*, 7306−7322.

(9) Yampolskii, Y. Polymeric gas separation membranes. *Macromolecules* **2012**, *45*, 3298−3311.

(10) Koros, W. J.; Fleming, G. K. Membrane-based gas separation. *J. Membr. Sci.* **1993**, *83*, 1−80.

(11) Robeson, L. M. Correlation of separation factor versus permeability for polymeric membranes. *J. Membr. Sci.* **1991**, *62*, 165−185.

(12) Robeson, L. M. The upper bound revisited. *J. Membr. Sci.* **2008**, *320*, 390−400.

(13) Stern, S. A. Polymers for gas separations: the next decade. *J. Membr. Sci.* **1994**, *94*, 1−65.

(14) Pera-Titus, M. Porous inorganic membranes for CO_2 capture: present and prospects. *Chem. Rev.* **2014**, *114*, 1413−1492.

(15) Gascon, J.; Kapteijn, F.; Zornoza, B.; Sebastián, V.; Casado, C.; Coronas, J. Practical approach to zeolitic membranes and coatings: state of the art, opportunities, barriers, and future perspectives. *Chem. Mater.* **2012**, *24*, 2829−2844.

(16) Ismail, A. F.; David, L. I. B. A review on the latest development of carbon membranes for gas separation. *J. Membr. Sci.* **2001**, *193*, 1−18.

(17) Shah, M.; McCarthy, M. C.; Sachdeva, S.; Lee, A. K.; Jeong, H. K. Current status of metal-organic framework membranes for gas separations: promises and challenges. *Ind. Eng. Chem. Res.* **2012**, *51*, 2179−2199.

(18) Qiu, S. L.; Xue, M.; Zhu, G. S. Metal-organic framework membranes: from synthesis to separation application. *Chem. Soc. Rev.* **2014**, *43*, 6116−6140.

(19) Yao, J. F.; Wang, H. T. Zeolitic imidazolate framework composite membranes and thin films: synthesis and applications. *Chem. Soc. Rev.* **2014**, *43*, 4470−4493.

(20) Kang, Z. X.; Xue, M.; Fan, L. L.; Huang, L.; Guo, L. J.; Wei, G. Y.; Chen, B. L.; Qiu, S. L. Highly selective sieving of small gas molecules by using an ultra-microporous metal-organic framework membrane. *Energy Environ. Sci.* **2014**, *7*, 4053−4060.

(21) Morigami, Y.; Kondo, M.; Abe, J.; Kita, H.; Okamoto, K. The first large-scale pervaporation plant using tubular-type module with zeolite NaA membrane. *Sep. Purif. Technol.* **2001**, *25*, 251−260.

(22) Chung, T. S.; Jiang, L. Y.; Li, Y.; Kulprathipanja, S. Mixed matrix membranes (MMMs) comprising organic polymers with dispersed inorganic fillers for gas separation. *Prog. Polym. Sci.* **2007**, *32*, 483−507.

(23) Dong, G. X.; Li, H. Y.; Chen, V. Challenges and opportunities for mixed-matrix membranes for gas separation. *J. Mater. Chem. A* **2013**, *1*, 4610−4630.

(24) Vinh-Thang, H.; Kaliaguine, S. Predictive models for mixed-matrix membrane performance: a review. *Chem. Rev.* **2013**, *113*, 4980−5028.

(25) Rezakazemi, M.; Amooghin, A. E.; Montazer-Rahmati, M. M.; Ismail, A. F.; Matsuura, T. State-of-the-art membrane based CO_2 separation using mixed matrix membranes (MMMs): an overview on current status and future directions. *Prog. Polym. Sci.* **2014**, *39*, 817−861.

(26) Bastani, D.; Esmaeili, N.; Asadollahi, M. Polymeric mixed matrix membranes containing zeolites as a filler for gas separation applications: a review. *J. Ind. Eng. Chem.* **2013**, *19*, 375−393.

(27) Moore, T. T.; Koros, W. J. Non-ideal effects in organic-inorganic materials for gas separation membranes. *J. Mol. Struct.* **2005**, *739*, 87−98.

(28) Jeazet, H. B. T.; Staudt, C.; Janiak, C. Metal-organic frameworks in mixed-matrix membranes for gas separation. *Dalton Trans.* **2012**, *41*, 14003−14027.

(29) Zornoza, B.; Tellez, C.; Coronas, J.; Gascon, J.; Kapteijn, F. Metal organic framework based mixed matrix membranes: an increasingly important field of research with a large application potential. *Microporous Mesoporous Mater.* **2013**, *166*, 67−78.

(30) Seoane, B.; Coronas, J.; Gascon, I.; Benavides, M. E.; Karvan, O.; Caro, J.; Kapteijn, F.; Gascon, J. Metal-organic framework based mixed matrix membranes: a solution for highly efficient CO_2 capture? *Chem. Soc. Rev.* **2015**, *44*, 2421−2454.

(31) Yang, T. X.; Xiao, Y. C.; Chung, T. S. Poly-/metal-benzimidazole nano-composite membranes for hydrogen purification. *Energy Environ. Sci.* **2011**, *4*, 4171−4180.

(32) Burtch, N. C.; Jasuja, H.; Walton, K. S. Water stability and adsorption in metal-organic frameworks. *Chem. Rev.* **2014**, *114*, 10575−10612.

(33) Côté, A. P.; Benin, A. I.; Ockwig, N. W.; O'Keeffe, M.; Matzger, A. J.; Yaghi, O. M. Porous, crystalline, covalent organic frameworks. *Science* **2005**, *310*, 1166−1170.

(34) Feng, X.; Ding, X. S.; Jiang, D. L. Covalent organic frameworks. *Chem. Soc. Rev.* **2012**, *41*, 6010−6022.

(35) Beaudoin, D.; Maris, T.; Wuest, J. D. Constructing monocrystalline covalent organic networks by polymerization. *Nat. Chem.* **2013**, *5*, 830−834.

(36) Zhang, Y. B.; Su, J.; Furukawa, H.; Yun, Y. F.; Gándara, F.; Duong, A.; Zou, X. D.; Yaghi, O. M. Single-crystal structure of a covalent organic framework. *J. Am. Chem. Soc.* **2013**, *135*, 16336−16339.

(37) Rowan, S. J.; Cantrill, S. J.; Cousins, G. R. L.; Sanders, J. K. M.; Stoddart, J. F. Dynamic covalent chemistry. *Angew. Chem., Int. Ed.* **2002**, *41*, 898−952.

(38) Ding, S. Y.; Wang, W. Covalent organic frameworks (COFs): from design to applications. *Chem. Soc. Rev.* **2013**, *42*, 548−568.

(39) Dogru, M.; Bein, T. On the road towards electroactive covalent organic frameworks. *Chem. Commun.* **2014**, *50*, 5531−5546.

DOI: 10.1021/acs.chemmater.5b02902
Chem. Mater. 2016, 28, 1277−1285

(40) Berlanga, I.; Ruiz-González, M. L.; González-Calbet, J. M.; Fierro, J. L. G.; Mas-Ballesté, R.; Zamora, F. Delamination of layered covalent organic frameworks. *Small* **2011**, *7*, 1207−1211.
(41) Berlanga, I.; Mas-Ballesté, R.; Zamora, F. Tuning delamination of layered covalent organic frameworks through structural design. *Chem. Commun.* **2012**, *48*, 7976−7978.
(42) Bunck, D. N.; Dichtel, W. R. Bulk synthesis of exfoliated two-dimensional polymers using hydrazone-linked covalent organic frameworks. *J. Am. Chem. Soc.* **2013**, *135*, 14952−14955.
(43) Chandra, S.; Kandambeth, S.; Biswal, B. P.; Lukose, B.; Kunjir, S. M.; Chaudhary, M.; Babarao, R.; Heine, T.; Banerjee, R. Chemically stable multilayered covalent organic nanosheets from covalent organic frameworks via mechanical delamination. *J. Am. Chem. Soc.* **2013**, *135*, 17853−17861.
(44) Chong, J. H.; Sauer, M.; Patrick, B. O.; MacLachlan, M. J. Highly stable keto-enamine salicylideneanilines. *Org. Lett.* **2003**, *5*, 3823−3826.
(45) Yang, T. X.; Shi, G. M.; Chung, T. S. Symmetric and asymmetric zeolitic imidazolate frameworks (ZIFs)/polybenzimidazole (PBI) nanocomposite membranes for hydrogen purification at high temperatures. *Adv. Energy Mater.* **2012**, *2*, 1358−1367.
(46) Lin, W. H.; Vora, R. H.; Chung, T. S. Gas transport properties of 6FDA-durene/1,4-phenylenediamine (pPDA) copolyimides. *J. Polym. Sci., Part B: Polym. Phys.* **2000**, *38*, 2703−2713.
(47) Lanni, L. M.; Tilford, R. W.; Bharathy, M.; Lavigne, J. J. Enhanced hydrolytic stability of self-assembling alkylated two-dimensional covalent organic frameworks. *J. Am. Chem. Soc.* **2011**, *133*, 13975−13983.
(48) Kandambeth, S.; Mallick, A.; Lukose, B.; Mane, M. V.; Heine, T.; Banerjee, R. Construction of crystalline 2D covalent organic frameworks with remarkable chemical (acid/base) stability via a combined reversible and irreversible route. *J. Am. Chem. Soc.* **2012**, *134*, 19524−19527.
(49) Biswal, B. P.; Chandra, S.; Kandambeth, S.; Lukose, B.; Heine, T.; Banerjee, R. Mechanochemical synthesis of chemically stable isoreticular covalent organic frameworks. *J. Am. Chem. Soc.* **2013**, *135*, 5328−5331.
(50) DeBlase, C. R.; Silberstein, K. E.; Truong, T. T.; Abruña, H. D.; Dichtel, W. R. β-Ketoenamine-linked covalent organic frameworks capable of pseudocapacitive energy storage. *J. Am. Chem. Soc.* **2013**, *135*, 16821−16824.
(51) Peng, Y. W.; Hu, Z. G.; Gao, Y. J.; Yuan, D. Q.; Kang, Z. X.; Qian, Y. H.; Yan, N.; Zhao, D. Synthesis of a sulfonated two-dimensional covalent organic framework as an efficient solid acid catalyst for biobased chemical conversion. *ChemSusChem* **2015**, *8*, 3208−3212.
(52) Li, Z. P.; Zhi, Y. F.; Feng, X.; Ding, X. S.; Zou, Y. C.; Liu, X. M.; Mu, Y. An azine-linked covalent organic framework: synthesis, characterization and efficient gas storage. *Chem. - Eur. J.* **2015**, *21*, 12079−12084.
(53) Stegbauer, L.; Hahn, M. W.; Jentys, A.; Savasci, G.; Ochsenfeld, C.; Lercher, J. A.; Lotsch, B. V. Tunable water and CO_2 sorption properties in isostructural azine-based covalent organic frameworks through polarity engineering. *Chem. Mater.* **2015**, *27*, 7874−7881.
(54) Addicoat, M. A.; Coupry, D. E.; Heine, T. AuToGraFS: automatic topological generator for framework structures. *J. Phys. Chem. A* **2014**, *118*, 9607−9614.
(55) Elstner, M.; Porezag, D.; Jungnickel, G.; Elsner, J.; Haugk, M.; Frauenheim, T.; Suhai, S.; Seifert, G. Self-consistent-charge density-functional tight-binding method for simulations of complex materials properties. *Phys. Rev. B: Condens. Matter Mater. Phys.* **1998**, *58*, 7260−7268.
(56) Nicolosi, V.; Chhowalla, M.; Kanatzidis, M. G.; Strano, M. S.; Coleman, J. N. Liquid exfoliation of layered materials. *Science* **2013**, *340*, 1226419.
(57) Ciesielski, A.; Samorì, P. Graphene *via* sonication assisted liquid-phase exfoliation. *Chem. Soc. Rev.* **2014**, *43*, 381−398.
(58) Peng, Y.; Li, Y. S.; Ban, Y. J.; Jin, H.; Jiao, W. M.; Liu, X. L.; Yang, W. S. Metal-organic framework nanosheets as building blocks for molecular sieving membranes. *Science* **2014**, *346*, 1356−1359.
(59) Ding, S. Y.; Gao, J.; Wang, Q.; Zhang, Y.; Song, W. G.; Su, C. Y.; Wang, W. Construction of covalent organic framework for catalysis: Pd/COF-LZU1 in Suzuki-Miyaura coupling reaction. *J. Am. Chem. Soc.* **2011**, *133*, 19816−19822.
(60) Zhao, D.; Yuan, D. Q.; Sun, D. F.; Zhou, H. C. Stabilization of metal-organic frameworks with high surface areas by the incorporation of mesocavities with microwindows. *J. Am. Chem. Soc.* **2009**, *131*, 9186−9188.
(61) Yuan, D. Q.; Zhao, D.; Sun, D. F.; Zhou, H. C. An isoreticular series of metal-organic frameworks with dendritic hexacarboxylate ligands and exceptionally high gas-uptake capacity. *Angew. Chem., Int. Ed.* **2010**, *49*, 5357−5361.
(62) Sumida, K.; Rogow, D. L.; Mason, J. A.; McDonald, T. M.; Bloch, E. D.; Herm, Z. R.; Bae, T. H.; Long, J. R. Carbon dioxide capture in metal-organic frameworks. *Chem. Rev.* **2012**, *112*, 724−781.
(63) Li, Z. P.; Feng, X.; Zou, Y. C.; Zhang, Y. W.; Xia, H.; Liu, X. M.; Mu, Y. A 2D azine-linked covalent organic framework for gas storage applications. *Chem. Commun.* **2014**, *50*, 13825−13828.
(64) Nugent, P.; Belmabkhout, Y.; Burd, S. D.; Cairns, A. J.; Luebke, R.; Forrest, K.; Pham, T.; Ma, S. Q.; Space, B.; Wojtas, L.; Eddaoudi, M.; Zaworotko, M. J. Porous materials with optimal adsorption thermodynamics and kinetics for CO_2 separation. *Nature* **2013**, *495*, 80−84.
(65) Myers, A. L.; Prausnitz, J. M. Thermodynamics of mixed-gas adsorption. *AIChE J.* **1965**, *11*, 121−127.
(66) Herm, Z. R.; Swisher, J. A.; Smit, B.; Krishna, R.; Long, J. R. Metal-organic frameworks as adsorbents for hydrogen purification and precombustion carbon dioxide capture. *J. Am. Chem. Soc.* **2011**, *133*, 5664−5667.
(67) Pesiri, D. R.; Jorgensen, B.; Dye, R. C. Thermal optimization of polybenzimidazole meniscus membranes for the separation of hydrogen, methane, and carbon dioxide. *J. Membr. Sci.* **2003**, *218*, 11−18.
(68) Jeong, H. K.; Krych, W.; Ramanan, H.; Nair, S.; Marand, E.; Tsapatsis, M. Fabrication of polymer/selective-flake nanocomposite membranes and their use in gas separation. *Chem. Mater.* **2004**, *16*, 3838−3845.
(69) Varoon, K.; Zhang, X. Y.; Elyassi, B.; Brewer, D. D.; Gettel, M.; Kumar, S.; Lee, J. A.; Maheshwari, S.; Mittal, A.; Sung, C. Y.; Cococcioni, M.; Francis, L. F.; McCormick, A. V.; Mkhoyan, K. A.; Tsapatsis, M. Dispersible exfoliated zeolite nanosheets and their application as a selective membrane. *Science* **2011**, *334*, 72−75.
(70) Rodenas, T.; Luz, I.; Prieto, G.; Seoane, B.; Miro, H.; Corma, A.; Kapteijn, F.; Xamena, F. X. L. I.; Gascon, J. Metal-organic framework nanosheets in polymer composite materials for gas separation. *Nat. Mater.* **2015**, *14*, 48−55.
(71) Kang, Z. X.; Peng, Y. W.; Hu, Z. G.; Qian, Y. H.; Chi, C. L.; Yeo, L. Y.; Tee, L.; Zhao, D. Mixed matrix membranes comprising two-dimensional metal-organic framework nanosheets for pre-combustion CO_2 capture: a relationship study of filler morphology versus membrane performance. *J. Mater. Chem. A* **2015**, *3*, 20801−20810.
(72) Perez, E. V.; Balkus, K. J.; Ferraris, J. P.; Musselman, I. H. Mixed-matrix membranes containing MOF-5 for gas separations. *J. Membr. Sci.* **2009**, *328*, 165−173.
(73) Ordoñez, M. J. C.; Balkus, K. J.; Ferraris, J. P.; Musselman, I. H. Molecular sieving realized with ZIF-8/Matrimid® mixed-matrix membranes. *J. Membr. Sci.* **2010**, *361*, 28−37.
(74) Vieth, W. R.; Howell, J. M.; Hsieh, J. H. Dual sorption theory. *J. Membr. Sci.* **1976**, *1*, 177−220.

DOI: 10.1021/acs.chemmater.5b02902
Chem. Mater. 2016, 28, 1277−1285